CHEMISTRY
A EUROPEAN JOURNAL

DOI: 10.1002/chem.200700865

Copper(II)-Mediated Aromatic *ortho*-Hydroxylation: A Hybrid DFT and Ab Initio Exploration

Peter Comba,* Stefan Knoppe, Bodo Martin, Gopalan Rajaraman, Claudio Rolli, Brett Shapiro, and Timon Stork[a]

Abstract: Mechanistic pathways for the aromatic hydroxylation by $[Cu^{II}(\mathbf{L^1})(TMAO)(O)]^-$ ($\mathbf{L^1}$ = hippuric acid, TMAO = trimethylamine *N*-oxide), derived from the O–N bond homolysis of its $[Cu^{II}(\mathbf{L^1})(TMAO)_2]$ precursor, were explored by using hybrid density functional theory (B3LYP) and highly correlated ab initio methods (QCISD and CCSD). Published experimental studies suggest that the catalytic reaction is triggered by a terminal copper–oxo species, and a detailed study of electronic structures, bonding, and energetics of the corresponding electromers is presented. Two pathways, a stepwise and a concerted reaction, were considered for the hydroxylation process. The results reveal a clear preference for the concerted pathway, in which the terminal oxygen atom directly attacks the carbon atom of the benzene ring, leading to the *ortho*-selectively hydroxylated product. Solvent effects were probed by using the PCM and CPCM solvation models, and the PCM model was found to perform better in the present case. Excellent agreement between the experimental and computational results was found, in particular also for changes in reactivity with derivatives of $\mathbf{L^1}$.

Keywords: ab initio calculations · copper · hydroxylation · reaction mechanisms · solvent effects

Introduction

The selective hydroxylation of aromatic compounds is one of the big challenges in synthetic organic chemistry and has gained considerable attention in recent years, particularly because hydroxylated aromatic compounds are important precursors in the pharmaceutical industry.[1] In nature metalloproteins with iron (pterin-dependent aromatic amino-acid hydroxylases and toluene mono-oxygenases) and copper-active centers (phenylalanine monoxygenase and tyrosinase) perform selective and efficient hydroxylation of aromatic rings.[2–7] A key to the understanding of the catalytic mechanism of these enzymes is the development of synthetic model compounds that mimic their catalytic activity, and a thorough investigation of their structural, electronic, and mechanistic properties.

There are a number of simple hydroxylation processes, such as reactions with H_2O_2 (H_2O_2–BF_3 or HF_3),[8] $KMnO_4$–H_2SO_4 mixtures,[9,10] $^{\bullet}OH$ radicals produced by X-ray radiolysis,[11] the classical or the modified Fenton's reactions,[9,12] the thermal decomposition of cupric salts of benzoic acid,[13,14] and the copper-mediated industrial production of phenol by the pyrolysis of benzoic acid in the Dow–Phenol process.[15–18] Many of these reactions have deficiencies in terms of efficiency and/or selectivity. Therefore, there is a continuous search for new catalyst systems with improved efficiency and selectivity.

The aromatic hydroxylation by iron enzymes is well established, and several active model compounds have been reported.[19–26] An interesting example is $[Fe(bpmen)(NCMe)_2]^{2+}$ (bpmen = *N*,*N*′-dimethyl-*N*,*N*′-bis(2-pyridylmethyl)ethane-1,2-diamine), which converts benzoic acid with H_2O_2 to salicylic acid with high selectivity (>90%) and efficiency.[27,28] The proposed mechanism features an electrophilic high-valence iron–oxo group as oxidant, and this is supported by experimental and theoretical work (note that catalysis by a $(HOO)Fe^{III}$-type species cannot be excluded[27]).[29] The putative Cu^{III}=O species, believed to be involved in copper-based catalytic cycles, is much less stable than the corresponding Fe^{IV}=O complexes that have been

[a] Prof. Dr. P. Comba, S. Knoppe, Dr. B. Martin, Dr. G. Rajaraman, C. Rolli, B. Shapiro, T. Stork
Universität Heidelberg, Anorganisch-Chemisches Institut
INF 270, 69120 Heidelberg (Germany)
Fax: (+49) 6226-548453
E-mail: peter.comba@aci.uni-heidelberg.de

Supporting information for this article is available on the WWW under http://www.chemeurj.org/ or from the author.

InterScience
© 2008 Wiley-VCH Verlag GmbH & Co. KGaA, Weinheim

characterized by spectroscopic and crystallographic analysis.[30–33]

The copper(II)-assisted *ortho*-hydroxylation of benzoic acid with trimethylamine *N*-oxide (TMAO, see Scheme 1) is an efficient and selective process.[34–38] The proposed mechanism (Scheme 2) involves coordination of Cu^{II} to the carboxylate group, followed by the oxidation with TMAO. This generates a highly reactive Cu^{II}–$O^{\bullet}$ or Cu^{III}=O intermediate that reacts with the adjacent benzyl group to produce the selectively *ortho*-hydroxylated products.[36] TMAO has been proposed as the source of oxygen, as the reaction does not evolve spontaneously and is inert towards atmospheric O_2, however, in association with TMAO, it produces the catalytically active species responsible for the hydroxylation process.[36] With the aim to thoroughly understand the mechanism and to probe the scope of the reaction, we have studied it with several benzoate derivatives (Scheme 3).[39] Only three of the seven ligands, $\mathbf{L}^{1-3}$, are catalytically active.

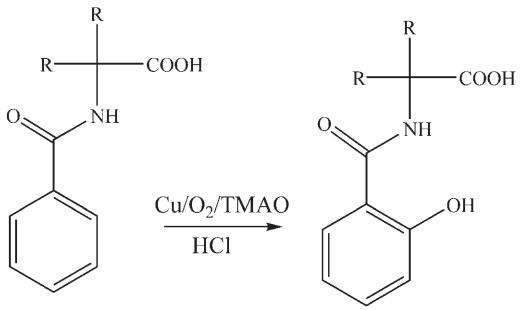

$\mathbf{L}^1$: R = H
$\mathbf{L}^2$: R = methyl
$\mathbf{L}^3$: R =phenyl

Scheme 1.

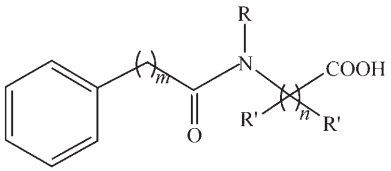

$\mathbf{L}^4$: R = Me; R' = Me; $n = 1$; $m = 0$
$\mathbf{L}^5$: R = H; R' = H; $n = 2$; $m = 0$
$\mathbf{L}^6$: R = H; R' = Me; $n = 1$; $m = 1$
$\mathbf{L}^7$: R = H; R' = Me; $n = 1$; $m = 2$

Scheme 3.

$\mathbf{L}^4$ has a methyl group at the amide nitrogen and $\mathbf{L}^{5-7}$ have longer spacer groups between either the amide and carboxylate or the amide and the benzene groups. These structural elements seem to prevent the formation of the copper complex, which is the putative resting state of the catalyst. The crystal-structure analysis of the copper(II) catalyst precursor and experiments with various derivatives of the ligand confirm that the formation of a copper–substrate–TMAO complex is essential for the catalytic reaction, and all experimental results support the formation of a Cu^{II}–$O^{\bullet}$ or a Cu^{III}=O complex as the catalytically active species.[39] This undergoes

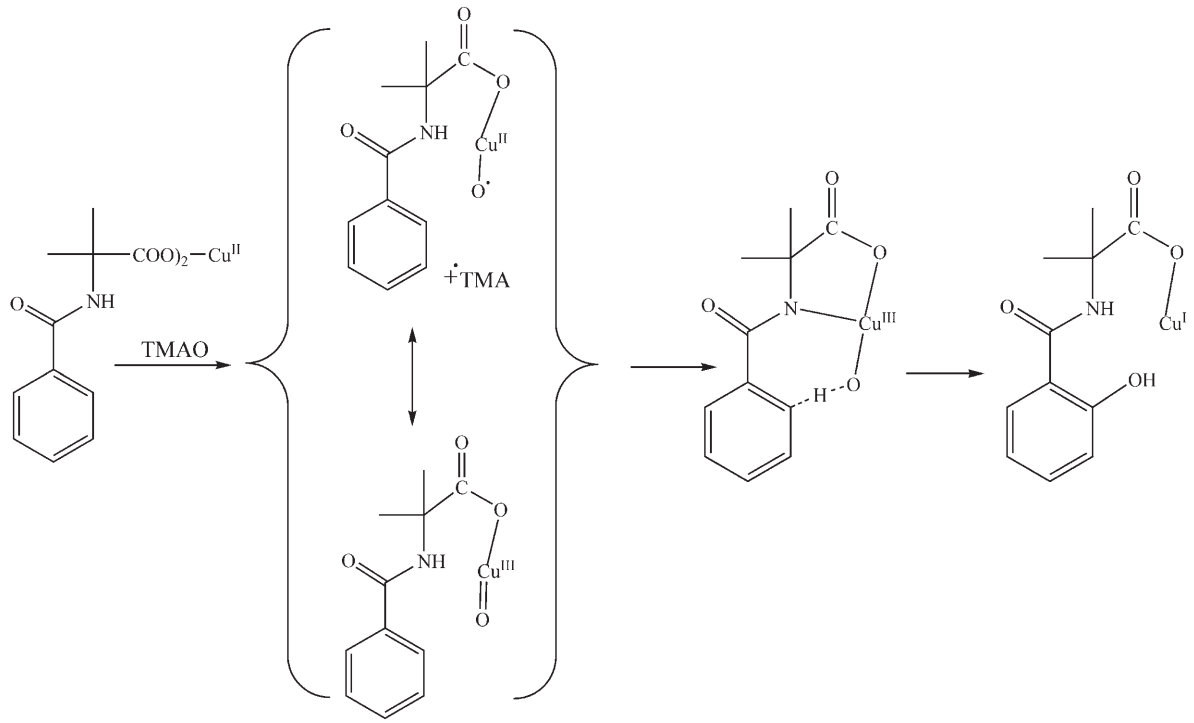

Scheme 2.

 © 2008 Wiley-VCH Verlag GmbH & Co. KGaA, Weinheim

intramolecular hydroxylation to yield selectively *ortho*-hydroxylated products. Despite extensive experimental studies, an evaluation of the bonding and reactivity of the terminal copper–oxo group seemed to be required to fully understand the catalytic cycle.

Here, we describe our results based on DFT and ab initio methods to explore the mechanism of the copper-mediated aromatic hydroxylation. Our main focus was the reactivity and the catalytic activity of the terminal copper–oxo intermediate, derived from the $[Cu^{II}(\mathbf{L^1})(TMAO)_2]$ complex. Copper–oxo groups are believed to be the catalytically active species in a number of biosystems, such as dopamine β-mono-oxygenase (DBM)[2,40,41] and methane mono-oxygenase,[42] and the energetics and mechanistic aspects discussed here might also provide a better understanding of the mechanism of these enzymes. The possible role of solvent in the process discussed here was investigated by using two different solvation models (PCM[43] and CPCM[44,45]). The validity of DFT methods, specifically that of the hybrid B3LYP functional, was addressed by performing calculations with high-level correlated methods and ab initio theory (QCISD[46] and CCSD[47–50]) for some species, and by comparing the trends of the computed and experimental data.

Computational Details

All calculations were performed by using the Gaussian 03[51] or Jaguar 5.5[52] suites of programs. The geometries were optimized by using the B3LYP functional.[53,54] Two different basis sets were used; BS I used in Jaguar 5.5 encompasses a double ζ-quality basis set with the Los Alamos effective core potential for Cu (commonly known as LanL2DZ[55–58] and a 6–31G basis set for the other atoms;[59] BS II used in the Gaussian suites of programs encompasses an Ahlrichs TZV basis set.[60,61] The single-point QCISD[46] and CCSD[47–50] calculations were performed with Gaussian 03 suite of programs on model complexes (see below), by using BS I on DFT-optimized geometries. Frequency calculations were performed on the optimized structures to verify that they are minima on the potential-energy surface (PES) and also to obtain zero-point energy corrections. The quoted DFT energies are B3LYP/TZV (BS II), including zero-point and free-energy corrections (enthalpy and entropy) from the frequency calculations at the temperature of 298.15 K, unless otherwise mentioned. For the location of transition states either the normal transition state search with a starting geometry obtained from B3LYP/BS I in Jaguar or the synchronous transit-guided quasi-Newton (STQN) method implemented in Gaussian 03 or a combination of both were used. The resulting optimized structures were verified as transition states by frequency calculations, and the single negative frequency was investigated visually by Molekel[62,63] to verify that the correct transition state was obtained.

The role of solvent on the structures and energetics was studied by reoptimization of some of the species at the B3LYP/BS II level with the polarizable continuum solvent model (PCM).[64–67] The conductor-like screening model (COSMO) implementation in Gaussian 03 (CPCM) was used for comparative purposes.[44,45] The UA0 (united atom model applied on atomic radii of the UFF force field) definition was used for the construction of the solute cavity. In the PCM solvent models studied the molecule is placed in a cavity, formed by overlapping atom-centered spheres, surrounded by a dielectric medium. The induced polarization of the environment is represented by point charges distributed on the surface of the cavity. In the CPCM model the solvent is described by a dielectric with the infinite permittivity, in which the polarization charges on the cavity surface are determined by supposing that the total electrostatic potential cancels out on the surface. Throughout the study acetonitrile was used as the solvent. For the transition states in the hydrogen-migration reaction, an individual sphere on the hydrogen atom of interest was used.

Results and Discussion

Based on the experimental observations, Scheme 4 was adopted for the DFT calculations. The DFT-optimized structure of $[Cu^{II}(\mathbf{L^1})(TMAO)_2]$ (^{2}**1** in Scheme 4) is shown in Figure 1a, and the computed parameters together with those from the X-ray analysis are collected in Table 1. The computed structure is in excellent agreement with the experimental data. The lengths of the two Cu–O bonds to the TMAO donors are significantly different, and this depends on the donor atom in the *trans* position. The geometry is approximately square planar, but the TMAO ligand *trans* to O3 significantly deviates from the O3-Cu-N1 plane. There is experimental evidence for the homolytic cleavage of the O–N bond in TMAO.[36] Terminal copper–oxo groups are believed to be involved in the catalytic cycles of the DBM and peptidylglycine-hydroxylating mono-oxygenase (PHM) families of copper mono-oxygenases as well as in the oxidation of methane by methane mono-oxygenase (MMO).[2,40–42] The active site of these enzymes possess different donor groups (typically histidines, methionine, and glutamate), but in all examples the copper centers are tetra-coordinated as in the complexes studied here. The homolytic cleavage of the O–N bond results in the formation a transient Cu^{II}–O$^{\bullet}$ (^{1,3}**2**) or Cu^{III}=O complex (^{1}**3**) that is believed to be the active species in the *ortho*-hydroxylation process.[68] These are the catalytically active species and also have significant biological relevance. Therefore, we first discuss in detail the structure, energetics and bonding of the possible electromers of Cu^{II}–O$^{\bullet}$, before we present our results of the reaction mechanism.

Electronic structure and bonding of Cu^{II}–O$^{\bullet}$ and Cu^{III}=O: The formation of terminal copper–oxo compounds by the spontaneous decomposition (the homolytic cleavage of the O–O bond) of μ-peroxo–dicopper(II) complexes has been reported.[69,70] It was shown that these transients are able to oxidize alkenes to the corresponding epoxides and to hydroxylated products.[69,70] However, there is no direct struc-

 © 2008 Wiley-VCH Verlag GmbH & Co. KGaA, Weinheim

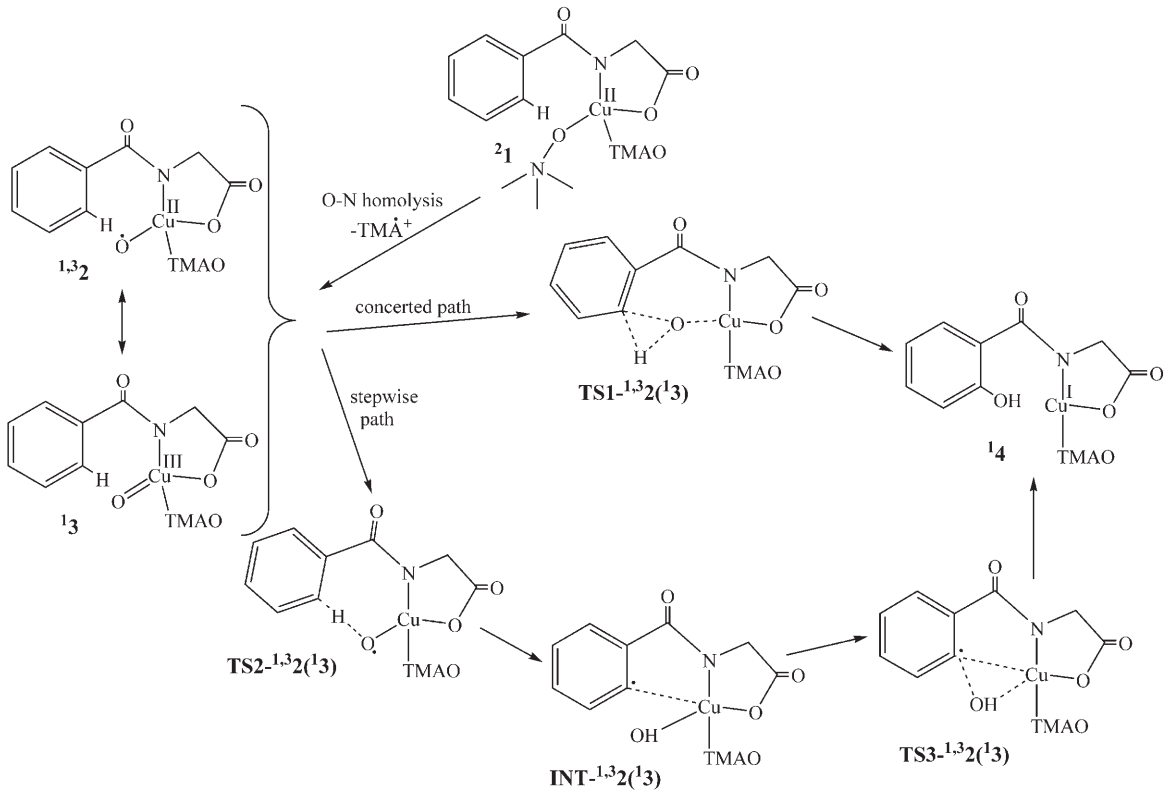

Scheme 4.

tural or spectroscopic evidence for ^{1,3}**2**- or ^{1}**3**-type compounds, which is attributed presumably to a very short lifetime due to a high reactivity, in particular also towards the formation of μ-oxo–dicopper(III) complexes.[2]

There are two electromeric forms of the terminal copper–oxo complex, a Cu^{II}–oxy radical **2** and the Cu^{III}–oxo species **3**. The two unpaired electrons in **2** are exchange coupled, resulting in the two possible total-spin ground states of $S=1$ (triplet) and $S=0$ (singlet). Due to the strict orthogonality condition met by two magnetic orbitals, the exchange interaction in **2** is expected to stabilize the triplet state.[71,72] The optimized structure of the triplet state of **2** (^{3}**2**) is shown in Figure 1b. Selected structural parameters for ^{3}**2** together with those of the structures of the corresponding singlet state ^{1}**2** and the singlet state of **3** (^{1}**3**) are given in Table 2. The electromer ^{3}**2** is found to be the ground state with ^{1}**2** being 16.1 kJ mol^{-1} and ^{1}**3** being 87.3 kJ mol^{-1} higher in energy.

The Cu–O1 bond in ^{3}**2** is significantly shorter than that in reactant ^{2}**1** (see Tables 1 and 2). The angle O1-Cu-O3 increases from 150.8 to 156.8°, and this moves the oxygen atom O1 into the copper–peptide plane. The distances between O1–C3 and O1–H1 are significantly shortened in the reactive species, which results in an ideal arrangement for the *ortho*-hydroxylation. The tetrahedral twist between the two planes N1-Cu-O3 and O1-Cu-O2 is 33.7 and 29.9° for ^{2}**1** and ^{3}**2**, respectively. The spin density on the copper atom of ^{3}**2** is delocalized to the donor atoms (the calculated Mulliken spin densities are collected in Table 3). The spin-density plot (Figure 1c) indicates that the unpaired electron on copper is in the d_{x2-y2} orbital and that of O1 is in one of the p orbitals.

The structural parameters of ^{3}**2** and ^{1}**2** are similar, except for the O1–C3 and O1–H1 distances, in which the former is significantly longer and the latter is shorter in the singlet state of **2**. This leads to a larger tetrahedral twist for the singlet-state structure (Table 2). Between ^{3}**2** and ^{1}**3** there are significant structural differences. Particularly, the Cu–O1 bond is very short in ^{1}**3** (1.752 vs. 1.886 Å), consistent with the expected double-bond character. The strength of the Cu–O bond in ^{1}**3** with respect to the two forms of **2** follows also from the stretching frequencies for the ^{1}**3** state (491 cm^{-1} for ^{3}**2**, 498 cm^{-1} for ^{1}**2**, and 656 cm^{-1} for ^{1}**3**). A qualitative molecular orbital (MO) diagram for ^{3}**2** and ^{1}**3** is shown in Figure 2, together with plots of the relevant DFT-computed molecular orbitals. There are two types of interactions between Cu^{II} and the oxy radical in ^{3}**2**. The one shown in Figure 2a has the unpaired electron on oxygen in a non-bonding orbital, and the closed-shell electrons interact with the d_{x2-y2} orbital, resulting in σ bonding and σ*-antibonding combinations. This leads to two unpaired electrons in the non-bonding oxygen and σ*-antibonding molecular orbitals, and these are orthogonal to each other and, therefore, stabilize the triplet state (note that C3 in the *ortho*-position has a significant contribution to this singly occupied molecular orbital (SOMO)). The singlet state ^{1}**2** can be accommodated

 © 2008 Wiley-VCH Verlag GmbH & Co. KGaA, Weinheim

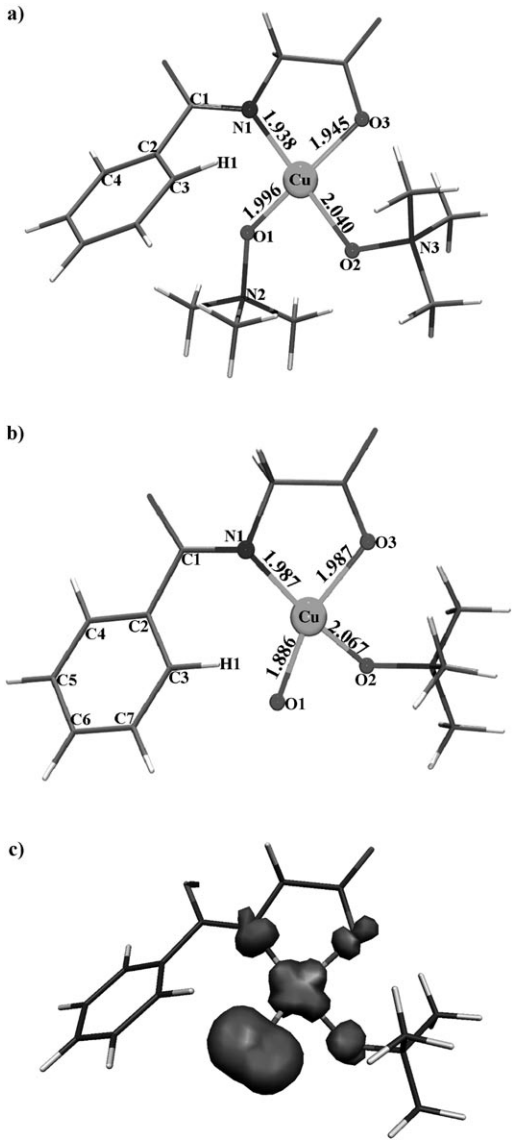

Figure 1. B3LYP-optimized structure of a) $[Cu^{II}(\mathbf{L^1})(TMAO)_2]$; b) the triplet state of $[Cu^{II}(\mathbf{L^1})(TMAO)(O)]^-$ ($^3\mathbf{2}$); c) spin-density plot of the triplet-state species $^3\mathbf{2}$. Bond lengths are given in Å; the α-spin density is given by the dark-grey shading.

in the same diagram with an opposite spin on the oxygen and the copper orbitals.

An additional π-type interaction between the singly occupied orbitals of oxygen and the doubly occupied orbitals of copper occurs in the $^1\mathbf{3}$ state. Here, the electrons are paired in the π-antibonding orbital, resulting in a Cu^{III}=O-type species.[73] As this π interaction involves the filled d_π orbital, it considerably destabilizes the Cu–O π-antibonding orbital.[74] The bonding situation is similar to that in the Fe^{IV}=O complexes, in which the stability is due to the available empty d orbitals for the π-type interaction. Due to the singly occupied orbitals and longer Cu–O distances **2** is expected to be a more powerful oxidant than **3**.

We now turn to the mechanism of the aromatic *ortho*-hydroxylation by $^{1,3}\mathbf{2}$ and $^1\mathbf{3}$. In the concluding sections we discuss the influence of solvation on the structures and energetics, compare the DFT data with ab initio (QCISD and CCSD) calculations, and finally compare the computed with experimental reactivities.

Table 1. Selected structural parameters of $[Cu^{II}(\mathbf{L^1})(TMAO)_2]$; experimental values are given in italics[42] (see Figure 1a for labeling).

Bond lengths [Å]		
Cu–O1	1.996	*1.955(1)*
Cu–O2	2.040	*1.928(1)*
Cu–O3	1.945	*1.945(1)*
Cu–N1	1.938	*1.928(1)*
O1–N2	1.467	*1.404(2)*
O2–N3	1.461	*1.406(2)*
O1–C3	3.532	*3.567*
O1–H1	3.719	*3.777*
Valence angles [°]		
N1-Cu-O1	94.5	*91.72(5)*
N1-Cu-O2	162.4	*160.78(6)*
N1-Cu-O3	84.5	*83.69(5)*
O1-Cu-O2	94.6	*95.88(5)*
O1-Cu-O3	150.8	*142.82(6)*
O2-Cu-O3	94.7	*100.41(5)*
Dihedral angles [°]		
Cu-N1-C1-C2	29.5	*31.55(2)*
N1-C1-C2-C3	39.5	*38.04(2)*
N1-C1-C2-C4	−145.8	*−146.87(2)*

Aromatic *ortho*-hydroxylation: Electrophilic versus H-abstraction pathways: The reactivity of the $^{1,3}\mathbf{2}$ and $^1\mathbf{3}$ species for the *ortho*-hydroxylation of aromatic compounds was studied by exploring the two alternative mechanisms of Scheme 4. In the concerted reaction the reactive species $^{1,3}\mathbf{2}$ or $^1\mathbf{3}$ activate the C–H bond in *ortho* position (C3; for labels, see Figure 1b), leading to **TS1** (Figure 3), which produces the *ortho*-hydroxylated product and copper(I). The alternative involves a stepwise pathway in which the C–H activation takes place when the terminal oxygen atom abstracts the benzylic hydrogen atom via **TS2** to produce a radical intermediate.[75,76] Here, we describe an intramolecular process in which only one of the orientations is possible. The hydroxylated product emerges then via **TS3**. The two pathways differ in the reactivity of the terminal oxygen atom. This is an important issue in the area of C–H activation by Cu^{II}–$O^\bullet$ groups in which catalysts with efficient hydrogen-abstraction capacity (stepwise pathway) and others that preferentially operate by electrophilic attack (concerted mechanism) are known.[41] The key results of the calculations related to the concerted reaction are shown in Figure 3 in which the optimized structures of **TS1**–$^3\mathbf{2}$ and the product $^1\mathbf{4}$ also are presented; the corresponding structural parameters are given in Table 2.

Although the triplet state is the ground state for **2**, the reactivity on the other surfaces ($^1\mathbf{2}$ and $^1\mathbf{3}$) was also considered (see Table 2 and Figure 3). The transition state **TS1** leads to an energy barrier of 34.9 kJ mol^{-1} on the $^3\mathbf{2}$ surface. The barriers for $^1\mathbf{2}$ and $^1\mathbf{3}$ are 47.6 and 123.3 kJ mol^{-1}, respectively.[77] The reaction is highly exothermic with a reaction energy of

 © 2008 Wiley-VCH Verlag GmbH & Co. KGaA, Weinheim

Table 2. Selected B3LYP-computed structural parameters for the reactants, transition states, intermediate, and product for the *ortho*-hydroxylation mechanism (see Figure 1b for labeling).

	^{3}**2**	^{1}**2**	^{1}**3**	**TS1–^{3}2**	**TS1–^{1}2**	**TS1–^{1}3**	**TS2–^{3}2**	**TS2–^{1}2**	**TS2–^{1}3**	**INT–^{3}2**	**TS3–^{3}2**	^{1}**4**
Bond lengths [Å]												
Cu–O1	1.886	1.885	1.752	1.906	1.905	1.791	1.907	1.907	1.831	1.950	1.964	3.157
Cu–O2	2.067	2.062	2.083	2.066	2.059	1.976	2.049	2.052	2.173	2.040	2.032	1.955
Cu–O3	1.987	1.985	1.972	1.999	1.988	1.960	1.990	1.981	1.984	2.102	1.957	2.185
Cu–N1	1.987	1.979	1.881	1.962	1.971	1.943	1.975	1.979	2.007	1.941	1.909	1.956
O1–C3	2.689	3.087	2.946	1.899	1.944	2.085	2.478	2.465	2.482	2.909	1.550	1.379
O1–H1	2.264	2.025	2.631	2.190	2.209	2.224	1.067	1.082	1.009	0.979	0.981	1.023
C3–H1				1.080	1.079	1.076	1.484	1.441	1.712	2.754	2.105	1.934
C2–C3				1.431	1.426	1.419	1.387	1.388	1.384	1.401	1.446	1.414
C2–C4				1.395	1.395	1.391	1.410	1.410	1.394	1.397	1.405	1.398
C3–C7				1.431	1.425	1.413	1.387	1.387	1.385	1.391	1.421	1.399
Valence angles [°]												
N1-Cu-O1	108.9	105.4	95.4	99.5	99.7	94.0	105.6	105.8	112.8	106.7	95.1	–
N1-Cu-O2	158.9	152.2	164.2	175.2	174.7	178.0	156.7	157.4	141.8	156.9	173.6	169.1
N1-Cu-O3	84.5	83.6	86.1	83.5	83.3	85.6	85.2	85.1	82.4	80.4	85.8	84.5
O1-Cu-O2	83.4	89.1	89.1	84.5	84.6	84.5	90.6	80.0	89.5	96.3	88.9	–
O1-Cu-O3	156.8	152.8	167.9	176.2	176.0	178.9	148.4	149.5	152.0	109.3	171.9	–
O2-Cu-O3	90.2	94.3	92.7	92.5	92.4	95.9	89.7	89.2	91.8	92.5	96.1	106.4
Cu-O1-C3				106.3	105.6	114.7	97.3	88.4	88.4	46.3	112.4	91.3
Cu-O1-H1				86.7	86.4	95.5	107.5	106.8	115.0	110.1	112.4	42.5
Dihedral angles [°]												
Cu-N1-C1-C2	23.6	−0.4	28.3	−19.2	−19.9	−28.6	2.6	2.9	−8.6	−2.0	10.8	58.1
N1-C1-C2-C3	36.7	29.5	20.1	−31.8	−32.4	−28.7	22.5	21.3	23.8	−0.3	5.9	30.0
N1-C1-C2-C4	−148.4	−151.9	−165.1	148.3	147.7	147.6	−159.3	−160.4	155.9	−179.0	179.0	156.6
Tetrahedral twist [°]												
∢N1-Cu-O3– ∢O1-Cu-O2	29.9	39.5	20.2	3.70	4.38	1.51	38.1	36.6	46.49	72.9	10.7	–

Table 3. Calculated spin densities of various species along the PES for the *ortho*-hydroxylation reaction (see Figure 1b for numbering).[a]

	^{3}**2**	^{1}**2**[a]	**TS1–^{3}2**	**TS1–^{1}2**	**TS2–^{3}2**	**TS2–^{1}2**	**INT–^{3}2**	**TS3–^{3}2**
Cu	0.554	0.585	0.546	0.556	0.588	0.600	0.721	0.647
O1	1.155	−0.831	0.825	−0.462	0.521	−0.245	0.398	0.069
O2	0.082	0.048	0.047	0.048	0.070	0.064	0.072	0.045
O3	0.059	0.071	0.053	0.059	0.065	0.070	0.049	0.100
N1	0.110	0.109	0.138	0.114	0.109	0.115	0.233	0.193
C1	−0.010	−0.003	−0.037	0.021	0.011	−0.024	−0.005	−0.004
C2	0.008	−0.005	0.282	−0.252	−0.003	0.008	0.027	0.117
C3	0.023	−0.010	−0.186	0.165	0.574	−0.569	0.393	0.521
C4	−0.006	0.001	−0.136	0.120	0.038	−0.039	0.019	−0.053
C5	0.015	0.001	0.263	−0.236	−0.022	0.023	−0.022	0.149
C6	−0.008	−0.001	−0.127	0.116	0.028	−0.031	0.023	0.051
C7	0.012	0.000	0.259	−0.235	−0.038	0.039	0.007	−0.009
H1	−0.015	0.016	0.034	−0.032	−0.004	0.008	−0.011	0.056

[a] The computed species from **^{1}3** have zero spin densities on all atoms.

184.2 kJ mol^{-1}. The C3–H1 distance in the transition state is not significantly elongated. An intrinsic reaction coordinate analysis (IRC) on the transition state reveals that the calculated transition state connects the two sides and, therefore, the process takes place in one rather than in multiple steps. A similar synchronous path for an aliphatic hydroxylation reaction from an IRC calculation has been observed for another mechanistic study with a bis(μ-oxo)dicopper(III) complex.[78] In the calculated transition state **TS1** the Cu–O1 bond is elongated relative to that of the reactant on all surfaces. The distances of the new interactions O1–C3 and O1–H1 increase in the order ^{3}**2** < ^{1}**2** < ^{1}**3**. Other salient structural features in the calculated transition state, in contrast to the reactants, are the distortion of the N1-Cu-O2 angle, the N1-C1-C2-C3 dihedral and the tetrahedral twist angle: all these parameters are related to the geometry of the chromophore, and this is close to perfectly square planar in the transition state. The larger energy barriers calculated on the ^{1}**2** and ^{1}**3** surfaces are essentially due to the energy difference of the reactants. The additional electronic and/or steric strain in the transition state on the different surfaces is within ≈5 kJ mol^{-1}. Note that the reactant has a triplet ground state and the product is a singlet. Therefore, a spin crossover after the formation of the transition state is predicted,[79–83] and this is favoured by spin-orbit coupling of the metal center.[84,85]

The spin-density distribution on the transition state **TS1–^{3}2** deserves some comment. The corresponding plot is shown in Figure 4a together with the two SOMOs (Figure 4b, c). The DFT-calculated spin-density values are given in Table 3. The absolute value of the spin density on the

 © 2008 Wiley-VCH Verlag GmbH & Co. KGaA, Weinheim

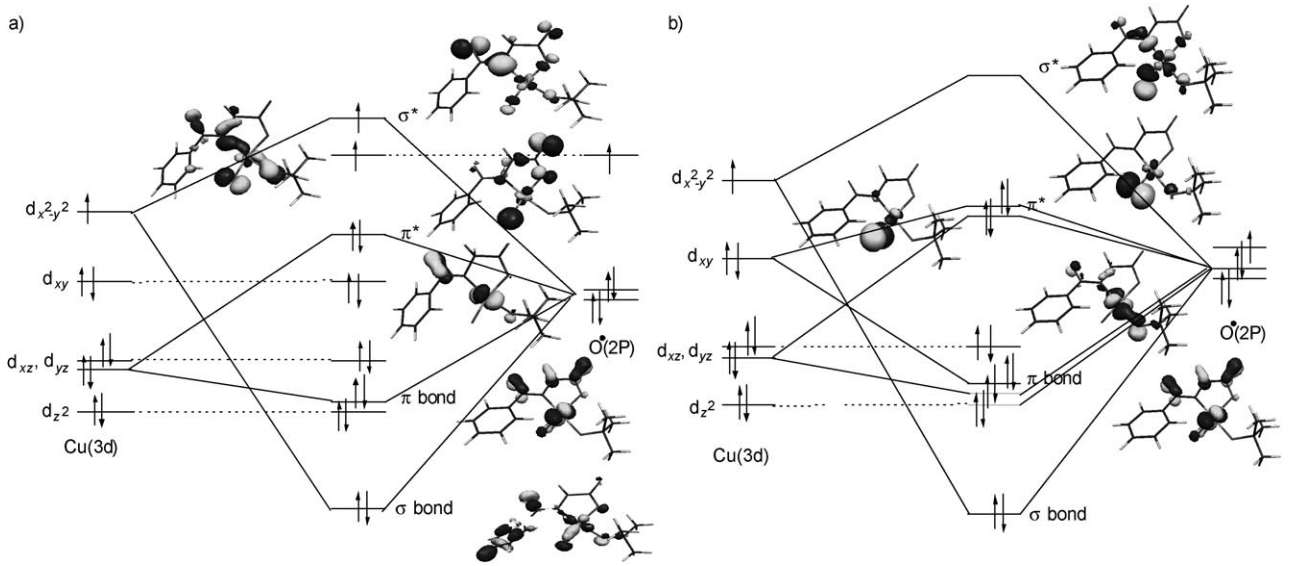

Figure 2. A qualitative MO diagram for a) ^{3}**2** and b) ^{1}**3**. The plotted molecular orbitals are derived from the B3LYP calculations.

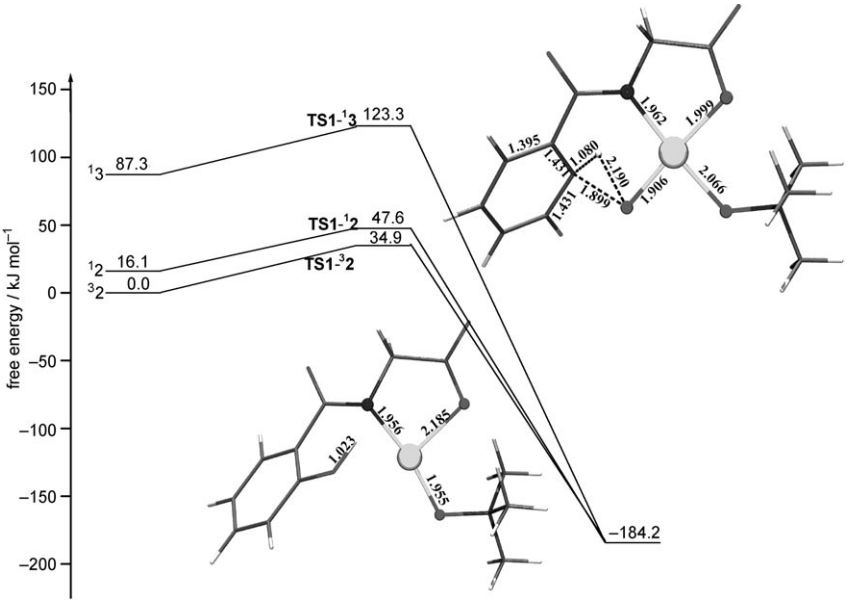

Figure 3. Computed-energy diagram for the concerted path of the *ortho*-hydroxylation mechanism. The results are summarized for all three states, ^{3}**2**, ^{1}**2**, and ^{1}**3**; the optimized structure of the transition state is that of **TS1**–^{3}**2**; bond lengths are given in Å; the imaginary frequencies are −495.2, −474.0, and −332.2 cm^{-1} for the ^{3}**2**, ^{1}**2**, and ^{1}**3** surfaces, respectively.

copper atom does not vary much across the row. However, the spin density on the oxygen atom that attacks the substrate is significantly reduced in the transition state **TS1**–^{3}**2**. The approach of O1 towards C3 transfers a significant amount of spin density from the carbon atom. This occurs through a spin-polarization mechanism, and the accumulated spin density on C3 has the opposite sign to that of O1 (Figure 4a and Table 3). The accumulated spin density on C3 propagates in the benzene ring through a dominant spin-polarization mechanism and, therefore, the neighbouring carbon atoms have alternate spin densities.

The potential-energy diagram along the reaction coordinate for the hydrogen-abstraction (stepwise) path is shown in Figure 5. The optimized structures of **TS2**–^{3}**2**, **INT**–^{3}**2**, and **TS2**–^{3}**2** are shown in Figure 6a–c, respectively. The calculated energy barrier for the transition state is 45.9 kJ mol^{-1} on the ^{3}**2** surface, and the formation of the intermediate is endothermic by 18.4 kJ mol^{-1}. The barrier heights on the ^{1}**2** and ^{1}**3** surfaces are 51.8 and 161.0 kJ mol^{-1}, respectively, relative to the ^{3}**2** ground state. In contrast to the concerted pathway, the transition states have different steric and electronic strain on the three spin surfaces. From the **TS2**–^{1}**3** transition state in particular emerges a very high energy barrier of 73.7 kJ mol^{-1}, that is, the ^{1}**3** reactant is a poor hydrogen acceptor. In the transition state, the C3–H1 bond is elongated and the O1–H1 bond is fully formed. The C3–H1 bond length and the barrier for **TS2** from the individual reactant increase in the order ^{1}**2** < ^{3}**2** < ^{1}**3**. The spin density of **TS2**–^{3}**2** (Figure 6d) on O1 is significantly smaller than that of the corresponding transition state in the concerted mechanism (0.521 vs. −0.825, Table 3). The C3 carbon atom has significant positive spin density. This is due to spin polarization, in which

 © 2008 Wiley-VCH Verlag GmbH & Co. KGaA, Weinheim

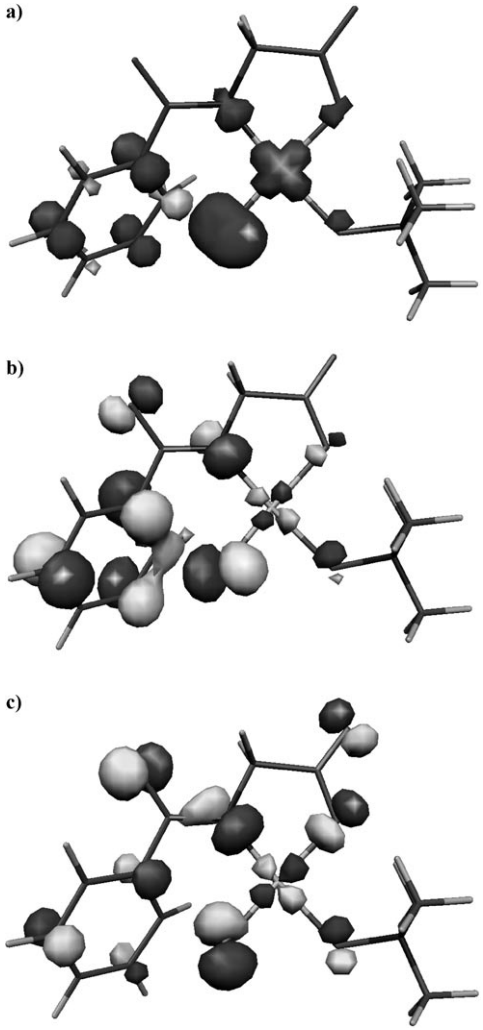

Figure 4. a) Spin-density plot of the transition state **TS1**–^{3}**2**; b, c) singly occupied orbitals of **TS1**–^{3}**2**; the α-spin density is given by the dark-grey shading and the β-spin density by the light-grey shading.

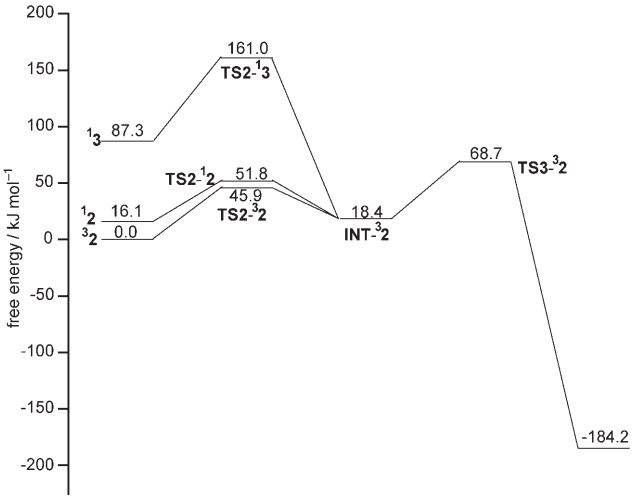

Figure 5. Computed-energy diagram for the stepwise path of the *ortho*-hydroxylation mechanism. The results are summarized for all three states, ^{3}**2**, ^{1}**2**, and ^{1}**3**, see text for details; the imaginary frequencies for **TS2** are −816.4, −663.5, and −427.4 cm^{-1} for the ^{3}**2**, ^{1}**2**, and ^{1}**3** surfaces, respectively, and for **TS3**–^{3}**2** it is −106.6 cm^{-1}.

the transferred hydrogen atom H1 gains negative spin density and induces an alternative sign for the spin density on carbon atom C3. In the aromatic ring the spin density is delocalized through spin polarization. In the **TS2**–^{1}**2** the spin density on O1 is half of that found in the triplet state (Table 3), but C3 has similar spin contributions on both spin surfaces.

Hydrogen abstraction leads to a radical center on the aromatic ring and the radical intermediate is stabilized by formation of a Cu–C interaction. Therefore, the intermediate on the ^{3}**2** surface has a square-pyramidal geometry (Figure 6b). The second transition state in the stepwise mechanism (**TS3**–^{3}**2**) has an energy barrier of 50.3 kJ mol^{-1} from the intermediate on the ^{3}**2** surface.[86] In **TS3**–^{3}**2** the new O1–C3 interaction is much stronger than in the concerted mechanism (1.550 vs. 1.899 Å), and the Cu–O1 interaction is elongated in preparation of the bond cleavage for the subsequent product formation. The reactant has a triplet ground state and the product is a singlet, and the spin crossover is expected to take place after the formation of the first transition state.

The barrier for the concerted mechanism is significantly smaller than the barriers on the ^{3}**2** surface of the stepwise pathway. The exothermicity of the formation of the radical intermediate and a substantial energy barrier for the second transition state indicate a kinetic as well as a thermodynamic preference for a concerted mechanism for the *ortho*-hydroxylation of benzoic acid derivatives. Clearly, Fe^{IV}=O complexes are structurally and electronically different from the Cu^{II}–O$^{\bullet}$ compounds discussed here. However, it is of interest that a recent experimental and theoretical study reveals that the Fe^{IV}=O unit in $[Fe^{IV}(N4Py)O]^{2+}$ (N4Py = *N*,*N*-bis(2-pyridyl)methylamine) performs hydroxylation through an electrophilic attack at the carbon atom. The lowest energy barrier from the quintet ground state in that study is 37.7 kJ mol^{-1}, and this is comparable to the computed barrier of 34.9 kJ mol^{-1} presented here for the concerted pathway.[29] Recently, aromatic hydroxylation by a mononuclear Cu^{II}–alkylperoxo complex has been reported.[87] The Cu^{II}–alkylperoxo complex was spectroscopically characterized and it has been shown that this complex gradually decomposes to another intermediate that is responsible for the hydroxylation reaction. Although structural information of that catalytically active species is not available, there is a possibility that it is related to the ^{3}**2** form discussed here. The observed kinetic deuterium-isotope effect supports the electrophilic-substitution pathway, and the estimated barrier height (enthalpy) of 24.9 ± 1.2 kJ mol^{-1} is in excellent agreement with the DFT-computed barrier (solvation effect included, see below) for the concerted pathway.[87]

Previous computational studies on the catalytic mechanism of dopamine β-mono-oxygenase (DBM) favor the hydrogen-abstraction mechanism by a Cu^{II}–O$^{\bullet}$ species for the

 © 2008 Wiley-VCH Verlag GmbH & Co. KGaA, Weinheim

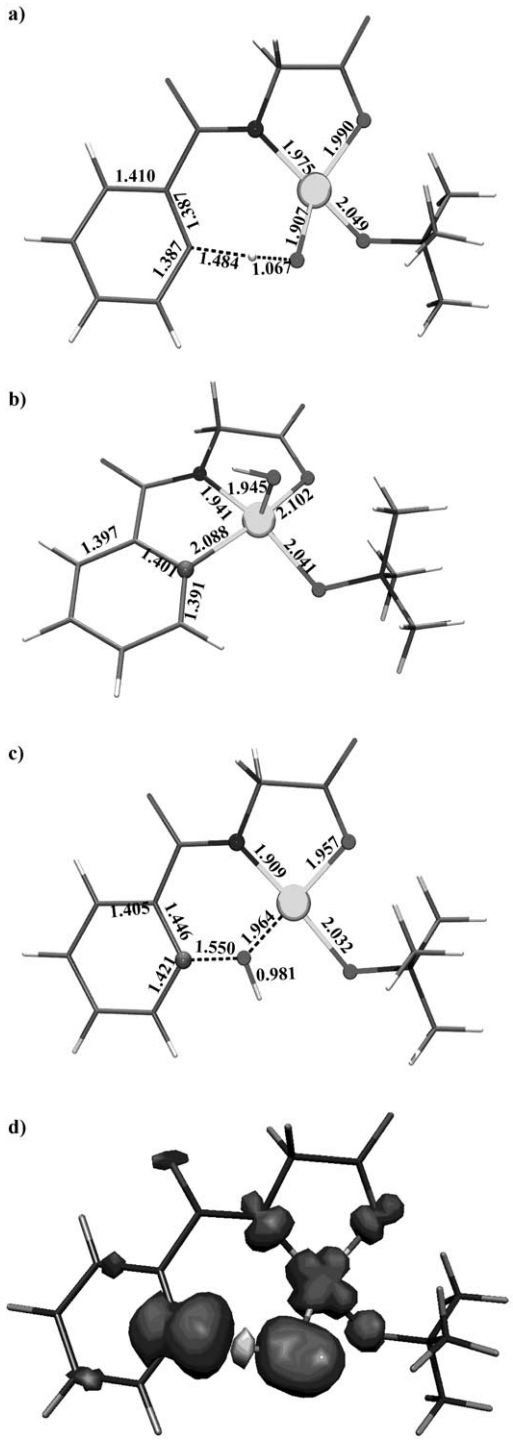

Figure 6. B3LYP-optimized structure of a) transition state **TS2**–^{3}**2**, b) intermediate **INT**–^{3}**2**, c) transition state **TS3**–^{3}**2**; d) spin-density plot of **TS2**–^{3}**2**. Bond lengths are given in Å and angles in degrees; the α-spin density is given by the dark-grey shading and the β-spin density by the light-grey shading.

C–H activation.[41] The calculated energy barrier for the first transition state on the triplet and singlet surfaces are only 3.3 and 15.9 kJ mol^{-1}, respectively.[41] The substantially lower energy barriers might be due to the different structure of the active site. However, and more importantly, the reported mechanism involves the activation of an aliphatic C–H bond. The radical intermediate in the DBM mechanism is exothermic by 83.7 kJ mol^{-1}. Similarly, the Cu^{II}–O$^{\bullet}$ species in methane mono-oxygenase,[42] in which the first energy barrier is 74.5 kJ mol^{-1}, and the radical intermediate is stabilized by 49.3 kJ mol^{-1}, also has favorable energetics for the hydrogen-abstraction path. From these studies it appears that the mechanism of C–H activation by terminal copper–oxo complexes primarily depends on the strength of the C–H bond. If it is aromatic it prefers an electrophilic attack at the carbon atom and for an aliphatic C–H activation, the hydrogen-abstraction pathway is preferred. Therefore, our mechanistic investigation provides an important insight into the reactivity of the terminal copper–oxo group, and the presented results have significant scope beyond our mechanistic issues.

Solvation effects on the mechanism of aromatic *ortho*-hydroxylation: Exploring the role of solvent in transition-metal-mediated reactions is a challenging task, especially if the geometries need to be reoptimized in the solvent phase.[88] Except for the calculations of redox potentials and absorption spectra,[89–92] the explicit consideration of solvent effects, for example, in mechanistic studies, with the full structural optimization of the solvated species, with either PCM or CPCM, is scarce.[93–95] The role of solvent is essential for our mechanistic study because the effect of the bulk solvent on the energetics of the reactant and transition states may favor one mechanism over another. Here, we have probed the solvent effects with two solvation models, that is, PCM and CPCM, for comparison. Selected structural parameters of the optimized structures of the reactants, transition states, and the product with solvation included, are given in Table 4.[96]

The calculated solvated structures are similar to those in the gas phase. Significant deviations include the O1–C3 and O1–H1 distances and the O1-Cu-O2 angle. In the solvated transition state the newly forming O–C bond is longer than that in the gas-phase geometry. Deviations between the two solvent models are small. In general, the calculated spin densities with solvent included are higher than those in the gas phase (Cu: 0.567 (PCM and CPCM) vs. 0.554 (vacuum) for ^{3}**2**), and this is consistent with earlier studies on copper proteins.[94] Solvation has also a significant effect on the energetics. The energy difference between the ^{3}**2** and ^{1}**3** electromers decreases to 64.7 kJ mol^{-1} with the PCM model and increases to 112.2 kJ mol^{-1} with the CPCM approach, from 87.3 kJ mol^{-1} in the gas phase. The energy barrier for the concerted transition state on the ^{3}**2** and ^{1}**3** surfaces are smaller than in the gas phase with the PCM solvation model (25.3 vs. 111.1 kJ mol^{-1}). However, the energy barrier on the ^{3}**2** surface is essentially unchanged with the CPCM model (34.9 vs. 34.2 kJ mol^{-1}).[97] The reaction energy is exothermic with 185.6 and 177.4 kJ mol^{-1} for the PCM and CPCM models, respectively. The energy barrier for the first transition state on the stepwise path is 39.7 kJ mol^{-1} with the

 © 2008 Wiley-VCH Verlag GmbH & Co. KGaA, Weinheim

Table 4. Selected B3LYP-computed structural parameters for the reactants, transition states, intermediate, and product for the *ortho*-hydroxylation mechanism using PCM and CPCM solvation models (see Figure 1b for labeling).

	^{3}**2**		^{1}**3**		**TS1–^{3}2**		**TS1–^{1}3**	**TS2–^{3}2**		^{1}**4**	
Bond lengths [Å]	PCM	CPCM	PCM	CPCM	PCM	CPCM	PCM	PCM	CPCM	PCM	CPCM
Cu–O1	1.889	1.890	1.783	1.784	1.919	1.919	1.812	1.907	1.915	3.199	3.193
Cu–O2	2.037	2.030	1.979	1.975	2.036	2.036	1.960	2.034	2.023	1.937	1.937
Cu–O3	1.980	1.996	1.989	1.986	2.010	2.010	1.964	1.981	1.989	2.233	2.237
Cu–N1	1.997	1.991	1.885	1.884	1.974	1.975		2.013	2.007	1.964	1.960
O1–C3	2.731	2.773	3.023	3.032	1.913	1.914	2.097	2.506	2.513	1.389	1.390
O1–H1	2.709	2.724	2.001	2.014	2.206	2.206	2.244	1.067	1.074	1.017	1.013
C3–H1					1.082	1.082	1.078	1.484	1.473	1.941	1.945
C2–C3					1.432	1.432	1.419	1.386	1.387	1.413	1.413
C2–C4					1.395	1.395	1.394	1.411	1.411	1.401	1.401
C3–C7					1.431	1.431	1.412	1.384	1.384	1.397	1.397
Valence angles [°]											
N1-Cu-O1	103.4	103.9	95.5	95.4	98.4	98.4	92.6	100.8	100.8	–	–
N1-Cu-O2	159.3	156.6	165.3	167.7	172.8	172.8	175.6	160.2	158.2	163.2	163.2
N1-Cu-O3	83.8	93.7	84.1	84.0	82.8	82.8	84.1	83.5	83.6	82.6	82.5
O1-Cu-O2	82.2	82.5	88.1	87.5	83.1	83.0	84.9	86.9	87.8	–	–
O1-Cu-O3	165.2	165.2	157.0	158.0	172.8	175.8	173.5	158.9	156.1	–	–
O2-Cu-O3	95.5	95.6	98.2	97.9	96.2	96.3	98.8	96.0	96.7	114.2	114.3
Cu-O1-C3					106.1	106.1	115.2	98.0	96.0	90.2	90.2
Cu-O1-H1					86.1	86.1	95.8	107.1	105.5	41.3	41.6
Dihedral angles [°]											
Cu-N1-C1-C2	24.7	25.2	−10.9	−11.2	−16.8	−16.4	−28.7	−3.8	−5.8	56.9	54.9
N1-C1-C2-C3	48.1	47.2	34.3	31.9	−32.9	−33.1	−30.4	27.6	28.1	32.5	33.8
N1-C1-C2-C4	−138.1	−139.3	−145.8	−147.8	147.2	147.0	146.5	−154.3	152.9	−154.2	−152.9

PCM and 49.3 kJ mol^{-1} with the CPCM models; here the PCM values are again lower than those in the gas phase, and the CPCM values are slightly higher.

As there is no significantly charged species involved, the reaction is expected to be accelerated in solution. Of the two solvation models the performance of the PCM approach is more satisfactory because the overall reaction is favored in solution, rather than in the gas phase. The reason for the contradictory energetics with the CPCM model are unclear, however, small deviations in the structures and the fact that this procedure may overestimate the entropic effects in the calculation of the free energy in solution might contribute.[98–100] Although the overall energetics change when solvation is included, the general trend remains the same: there is a preference for the concerted over the stepwise mechanism.

Reliability of DFT methods—comparison with QCISD and CCSD methods: The mechanism studied here involves open-shell molecules and possesses multi-determinant characteristics. Therefore, it is important to evaluate carefully the choice of DFT method. The performance of the hybrid B3LYP functional for this kind of study is well documented.[101–109] However, there are cases in which B3LYP fails to predict the correct spin-state ordering in contrast to high-level CASPT2 calculations.[107] A study of particular relevance to that discussed here is the failure of DFT (BLYP) to predict the correct ground state of the copper(III) peroxide–copper(II) superoxide continuum in mononuclear copper complexes with a β-diketiminate ligand backbone:[110] BLYP predicts a triplet as the ground state, whereas CASPT2 calculations reveal that the true ground state is a singlet over a range of Cu–O distances. The discrepancies in energetics between the two levels in this particular case is as high as 90 kJ mol^{-1} (note that the comparison has been made with the BLYP functional, which is known to disfavor the singlet state much more than the hybrid B3LYP functional).[111] In most cases the expected errors due to B3LYP calculations are in the range of 10–20 kJ.[112]

Because DFT calculations have been shown to fail to predict the ground state for systems with biradical character, it is essential at this point to test the performance of DFT (B3LYP) for our system, as our complexes also have a biradical-like behavior and the energy differences calculated by DFT for ^{3}**2** and ^{1}**3** are within the 90 kJ mol^{-1} error margin discussed above.[110] Although multi-configuration CI calculations (especially CASSCF and CASPT2) are the methods of choice for this kind of investigation, they are problematic due to the size of the systems of interest because they normally require a very large active space for high quality results.[113–115] Additionally, the calculation of transition states for such large molecules with CASPT2 is beyond scope. Therefore, we have adopted QCISD and CCSD calculations (without the connected triples) for our benchmarking. Both the QCISD and the variant of CCSD methods are size consistent, and there are few instances in which CCSD is found to be superior to the QCISD methodology.[116–118] Therefore, we have adopted both approaches to validate the methods used for our mechanistic studies. Both methods are computationally very demanding and, therefore, some compromis-

 © 2008 Wiley-VCH Verlag GmbH & Co. KGaA, Weinheim

es (to energetics and accuracy) have been made: 1) The complexes were simplified to $[Cu(\mathbf{L^1})(O)(NH_3)]^-$ and 2) only single-point calculations using BSI at the B3LYP/BSI geometry on the selected species have been performed.[119]

The CCSD and the QCISD calculations yield $^3\mathbf{2}$ to $^1\mathbf{3}$ energy gaps of 95.9 and 67.2 kJ mol^{-1}, respectively, compared to the B3LYP value of 83.7 kJ mol^{-1}. This result itself is interesting because the QCISD and CCSD calculations vary by approximately 29 kJ mol^{-1} and the B3LYP results are rather close to the CCSD value. Because in several studies CCSD calculations have been shown to be superior to QCISD calculations,[116–118] it is tempting to assume that the QCISD calculations underestimate the $^3\mathbf{2}$–$^1\mathbf{3}$ energy gap while the B3LYP results are acceptable. The calculated energy barrier for **TS1**–$^3\mathbf{2}$ is 48.7 kJ mol^{-1} (QCISD) and 49.0 kJ mol^{-1} (CCSD), compared to that of 30.4 kJ mol^{-1} by DFT. The QCISD and CCSD calculations yield a reaction energy of −194.7 and −152.7 kJ mol^{-1}, respectively, compared to that of −203.9 kJ mol^{-1} by DFT. That is, the calculated energy barrier of both ab initio methods is the same and the DFT calculations underestimate the barrier height and slightly overestimate the reaction energy, compared to the ab initio results.

Selected Mulliken spin densities, calculated with all three methods, are given in Table 5. For the $^3\mathbf{2}$ species the spin density on the copper atom calculated using the CCSD and QCISD methods is significantly higher and that on O1 is lower than those calculated by DFT methods. This is due to the well-known overestimation by DFT calculations of the covalency in Cu^{II} complexes.[120–123] A similar situation is observed for **TS1**–$^3\mathbf{2}$. Surprisingly, the spin density on carbon atom C3 (and all other benzylic carbon atoms through spin polarization) is much higher than that calculated with B3LYP (−0.930 vs. −0.210).

Table 5. A comparison between the CCSD-, QCISD-, and B3LYP-calculated spin densities of selected species on the PES for the *ortho*-hydroxylation reaction (see Figure 1b for numbering).[a]

	$^3\mathbf{2}$[a]			**TS1**–$^3\mathbf{2}$		
	CCSD	QCISD	B3LYP	CCSD	QCISD	B3LYP
Cu	0.816	0.816	0.489	0.821	0.821	0.493
O1	1.085	1.085	1.204	0.923	0.922	0.890
C2	−0.033	−0.033	0.020	0.970	0.970	0.299
C3	0.047	0.047	0.002	−0.930	−0.930	−0.210
C4	0.039	0.039	−0.011	−0.915	−0.915	−0.166
C5	−0.035	−0.034	0.018	0.969	0.969	0.277
C6	0.039	0.039	−0.010	−0.899	−0.899	−0.155
C7	−0.034	−0.035	0.016	0.953	0.952	0.290
H1	−0.014	−0.013	−0.006	0.085	0.085	0.029

[a] The computed species from the $^1\mathbf{3}$ have zero spin densities on all atoms.

Although the B3LYP calculations provide a reliable singlet–triplet gap ($^3\mathbf{2}$–$^1\mathbf{3}$), compared to the CCSD method, there are discrepancies between the two methodologies in the calculated energy-barrier height on the triplet surface and the computed reaction energy. This may be due partly to the B3LYP functional.[124–126] However, a quantitative comparison cannot be made as this would require the use of higher basis sets for the CCSD and QCISD calculations and such calculations are beyond our computational resources.[127] In general, the higher-level results (QCISD and CCSD) are qualitatively comparable to those with B3LYP. To this end, we conclude that, within the expected error limit, the B3LYP functional is the method of choice for large transition-metal-ion complexes.

Relevance to experimental results: Effects of ligand substitution on the reactivity: There are no kinetic results to estimate the height of the energy barrier of the reaction for comparison with the computational results. However, the present theoretical data can be compared with the experimental results of the aromatic hydroxylation with differently substituted ligands. Among the several ligand systems, studied $\mathbf{L^1}$, $\mathbf{L^2}$, and $\mathbf{L^3}$ (Scheme 1 and 3) are catalytically active for the *ortho*-hydroxylation. The most active catalyst is based on $\mathbf{L^2}$ and the ratio of *ortho*-hydroxylation after a reaction time of 24 h is 35.2% ($\mathbf{L^1}$), 46.8% ($\mathbf{L^2}$), and 25.6% ($\mathbf{L^3}$). Therefore, the experiments reveal a reactivity pattern of $\mathbf{L^2} > \mathbf{L^1} > \mathbf{L^3}$.[39]

The DFT results for the systems with $\mathbf{L^2}$ and $\mathbf{L^3}$ are summarized in Figure 7, and important structural parameters

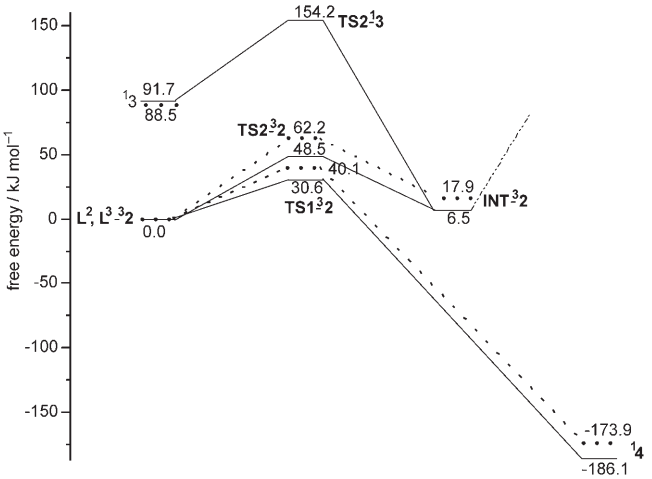

Figure 7. Computed-energy diagram of the concerted and stepwise paths for the *ortho*-hydroxylation mechanism with the $\mathbf{L^2}$- and $\mathbf{L^3}$-based complexes; solid lines are for $\mathbf{L^2}$ and dotted lines for $\mathbf{L^3}$. The imaginary frequencies are, for **TS1**: −478.4 cm^{-1} on the $^3\mathbf{2}$ surface for the $\mathbf{L^2}$ and $\mathbf{L^3}$ complexes; for **TS2**: −548.0 and −815.4 cm^{-1} on the $^3\mathbf{2}$ surface for the $\mathbf{L^2}$ and $\mathbf{L^3}$ complexes, respectively; for **TS2**–$^1\mathbf{3}$: −480.2 cm^{-1} for the $\mathbf{L^2}$ complex.

are given in Table 6. The ground state in both cases is $^3\mathbf{2}$, and the energy difference between the $^3\mathbf{2}$ and $^1\mathbf{3}$ is 88.5 and 91.7 kJ mol^{-1} for $\mathbf{L^2}$ and $\mathbf{L^3}$, respectively. Concerted and stepwise paths were considered, and in both cases **TS1**–$^3\mathbf{2}$ is found to be lower in energy than **TS2**–$^3\mathbf{2}$. The calculated energy-barrier heights are 30.6 and 40.1 kJ mol^{-1} for the $\mathbf{L^2}$-

 © 2008 Wiley-VCH Verlag GmbH & Co. KGaA, Weinheim

Table 6. Selected B3LYP-computed geometric parameters for the reactants, transition states, and intermediate, of the *ortho*-hydroxylation mechanism for $\mathbf{L^2}$ and $\mathbf{L^3}$ copper complexes (see Figure 1b for labeling).

	^{3}**2**		^{1}**3**		**TS1**–^{3}**2**		**TS2**–^{3}**2**	
Bond lengths [Å]	$\mathbf{L^2}$	$\mathbf{L^3}$	$\mathbf{L^2}$	$\mathbf{L^3}$	$\mathbf{L^2}$	$\mathbf{L^3}$	$\mathbf{L^2}$	$\mathbf{L^3}$
Cu–O1	1.885	1.884	1.773	1.776	1.900	1.896	1.885	1.908
O1–C3	2.667	2.411	3.138	3.333	1.903	1.902	2.461	2.450
O1–H1	2.565	2.650	3.360	3.583	2.213	2.214	1.053	1.078
C3–H1								
Bond angles [°]								
N1-Cu-O2	158.3	158.9	173.6	174.4	175.4	171.5	156.6	153.0
N1-C1-C2-C3	39.1	40.0	42.3	38.3	−33.0	−0.2	35.6	26.8

and $\mathbf{L^3}$-based copper(II) complexes, respectively. As with $\mathbf{L^1}$, the reaction is highly exothermic with a reaction energy of 186.1 and 173.9 kJ mol^{-1} for the $\mathbf{L^2}$- and $\mathbf{L^3}$-based systems, respectively. The stepwise path is higher in energy with a **TS2**–^{3}**2** barrier of 48.5 and 62.2 kJ mol^{-1} for the $\mathbf{L^2}$- and $\mathbf{L^3}$-based systems. The formation of the intermediate is endothermic in both cases (6.5 and 17.9 kJ mol^{-1} for the $\mathbf{L^2}$- and $\mathbf{L^3}$-based systems). Assuming that the reaction in $\mathbf{L^{1-3}}$ occurs through a concerted mechanism, the energy barrier decreases and the exothermicity of the reaction increases in the order $\mathbf{L^2} > \mathbf{L^1} > \mathbf{L^3}$, that is, as observed experimentally.[39] The calculated product ratio, based on the barrier heights of the concerted transition state alone (100($\mathbf{L^2}$):88($\mathbf{L^1}$):76($\mathbf{L^3}$)) is in good agreement with the experimentally observed product ratio (100($\mathbf{L^2}$):75($\mathbf{L^1}$):54($\mathbf{L^3}$)). That is, the reactivity pattern predicted by DFT is in excellent agreement with the experimental observations.[36,39]

Another set of calculations, for which a comparison to experiment can be made is the N1-C1-C2-C3 dihedral angle in ^{3}**2**. When 3′-fluoro-substituted benzamide is used, the hydroxylation produces both *ortho*- and *para*-hydroxylated products with respect to the fluorine substituent. The estimated *ortho*/*para* ratio is 0.41.[36] The formation of the two products reveals that the energy required for rotation of the N1-C1-C2-C3 dihedral angle should be smaller than the computed barrier height for the concerted path. To validate this prediction, a relaxed potential-energy scan on ^{3}**2** was performed at the B3LYP/BSI level by varying the N1-C1-C2-C3 dihedral angle from 36.7 to 156.7°. This scan (Figure 8) yields as upper limit of the rotational-energy barrier 19.0 kJ mol^{-1}, that is, a value that is smaller than the calculated energy barrier of the concerted pathway (45.9 kJ mol^{-1}), and, therefore, is consistent with the experimental observations.[36]

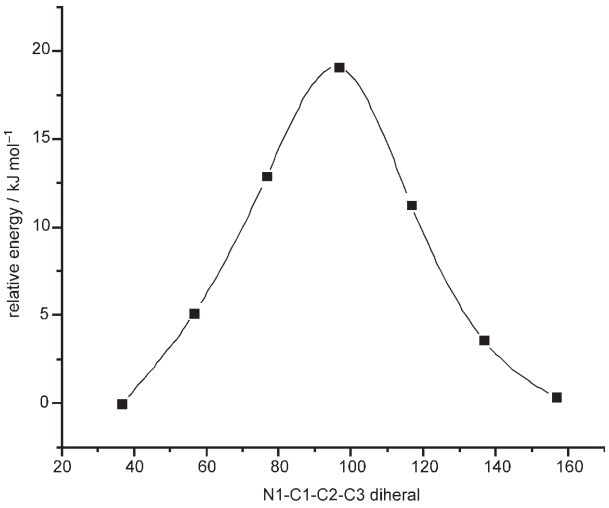

Figure 8. Relaxed potential-energy scan for the N1-C1-C2-C3 dihedral-angle rotation in ^{3}**2**; see Figure 1a for labeling.

Conclusions

The results of density functional theory (B3LYP) and ab initio (QCISD and CCSD) calculations were used to understand the mechanism of aromatic hydroxylation by a transient terminal copper–oxo complex. Calculations with different levels of sophistication to incorporate electron correlation consistently reveal the triplet state as the ground state for Cu^{II}–O$^{\bullet}$. The closed-shell singlet Cu^{III}=O is, due to its instability, caused by a weak π interaction between the filled metal d_π and the oxygen p orbital, too high in energy to be involved in C–H activation. Two pathways were considered; a concerted mechanism in which the terminal oxygen atom attacks the benzene ring and captures the benzylic hydrogen atom, and a stepwise process in which the hydrogen transfer occurs in two steps. Both pathways are regioselective with respect to the *ortho* position and all calculations consistently favor the concerted pathway. Although the barrier height for the first transition state in the stepwise path is only ≈10 kJ mol^{-1} higher than that of the more favorable concerted reaction, the severe energy penalty involved in the formation of the radical intermediate and the high energy of the second transition state indicate that the stepwise pathway may be excluded for the aromatic hydroxylation process. Solvation does not change this trend and the calculated barrier height of 25.3 kJ mol^{-1} with the PCM method is in excellent agreement with the experimental barrier (24.9 ± 1.2 kJ mol^{-1}) reported for the aromatic hydroxylation reaction by a copper species.[87] Calculations on various ligand derivatives demonstrate the influence of substituents on the reactivity. The trends observed by experiment are fully supported by the DFT calculations.[39] Our mechanistic studies also shed some light on the reactivity of the two faces of Cu^{II}–O$^{\bullet}$, which activates aromatic C–H bonds by a concerted path and aliphatic C–H bonds by a stepwise mechanism.

 © 2008 Wiley-VCH Verlag GmbH & Co. KGaA, Weinheim

Acknowledgement

Financial support by the German Science Foundation (DFG) and an AvH fellowship to G.R. are gratefully acknowledged.

[1] R. A. Sheldon, J. K. Kochi, *Metal-Catalyzed Oxidations of Organic Compounds*, Academic Press, New York, **1981**.
[2] Y. Lee, K. D. Karlin in *Concepts and Models in Bioinorganic Chemistry* (Eds.: H.-B. Kraatz, N. Metzler-Nolte), Wiley-VCH, Weinheim, **2006**.
[3] R. Ullrich, M. Hofrichter, *Cell. Mol. Life Sci.* **2007**, *64*, 271.
[4] O. Toussaint, K. Lerch, *Biochemistry* **1987**, *26*, 8567.
[5] L. Q. Hatcher, K. D. Karlin, *J. Biol. Inorg. Chem.* **2004**, *9*, 669.
[6] E. A. Lewis, W. B. Tolman, *Chem. Rev.* **2004**, *104*, 1047.
[7] L. M. Mirica, X. Ottenwaelder, T. D. P. Stack, *Chem. Rev.* **2004**, *104*, 1013.
[8] K.-F. Wedemeyer in *Methoden der Organischen Chemie* (Eds. J. Houben, T. Weyl), Georg Thieme Verlag, Stuttgart, **1976**, p. 4.
[9] S. Udenfried, C. T. Clark, A. J. B. Brodie, *J. Biol. Chem.* **1954**, *208*, 731.
[10] A. Leman, M. T. Montaigne, *Acad. Sci.* **1950**, *231*, 412.
[11] H. Loebl, G. Stein, J. Weiss, *J. Chem. Soc.* **1951**, 405.
[12] H. J. H. Fenton, *J. Chem. Soc.* **1894**, *65*, 899.
[13] W. W. Kaeding, G. R. Colling, *J. Org. Chem.* **1965**, *30*, 3750.
[14] W. W. Kaeding, A. T. Shulgin, *J. Chem. Soc.* **1953**, *288*, 3551.
[15] W. Buijs, *DSM Res. Commun.* **1993**, *4*.
[16] W. Buijs, *J. Mol. Catal. A* **1999**, *146*, 237.
[17] W. Buijs, P. Comba, D. Corneli, Y. Mengerink, H. Pritzkow, M. Schickedanz, *Eur. J. Inorg. Chem.* **2001**, 3143.
[18] G. S. Bull, G. H. Searle, *J. Chem. Educ.* **1986**, *63*, 902.
[19] S. J. Lange, H. Miyake, L. Que, Jr., *J. Am. Chem. Soc.* **1999**, *121*, 6330.
[20] M. P. Jensen, S. J. Lange, M. P. Mehn, L. E. Que, L. Que, Jr., *J. Am. Chem.Soc.* **2003**, *125*, 2113.
[21] N. Kitajima, M. Ito, H. Fukui, Y. Moro-oka, *J. Am. Chem. Soc.* **1993**, *115*, 9335.
[22] T. Funabiki, T. Yokomizo, S. Suzuki, S. Yoshida, *Chem. Commun.* **1997**, 151.
[23] S. Menage, J.-B. Galey, J. Dumats, G. Hussler, M. Seite, I. G. Luneau, G. Chottard, M. Fontecave, *J. Am. Chem. Soc.* **1998**, *120*, 13370.
[24] Y. Mekmouche, S. Menage, C. Toia-Duboc, M. Fontecave, J.-B. Galey, C. Lebrun, J. Pecaut, *Angew. Chem.* **2001**, *113*, 975; *Angew. Chem. Int. Ed.* **2001**, *40*, 949.
[25] M. P. Mehn, K. Fujisawa, E. L. Hegg, L. Que, Jr., *J. Am. Chem. Soc.* **2003**, *125*, 7828.
[26] F. Avenier, J. L. DuBois, J.-M. Latour, *New J. Chem.* **2004**, *28*, 782.
[27] S. Taktak, M. Flook, B. M. Foxman, L. Que, Jr., E. V. Rybak-Akimova, *Chem. Commun.* **2005**, 5301.
[28] N. Y. Oh, M. S. Seo, M. H. Lim, M. B. Consugar, M. J. Park, J.-U. Rohde, J. Han, K. M. Kim, J. Kim, L. Que, Jr., W. Nam, *Chem. Commun.* **2005**, 5644.
[29] S. P. De Visser, K. Oh, A.-R. Han, W. Nam, *Inorg. Chem.* **2007**, *46*, 4632.
[30] E. I. Solomon, T. C. Brunold, M. I. Davis, J. N. Kemsley, S.-K. Lee, N. Lehnert, F. Neese, A. J. Skulan, Y.-S. Yang, J. Zhou, *Chem. Rev.* **2000**, *100*, 235.
[31] M. Costas, M. P. Mehn, M. P. Jensen, L. Que, Jr., *Chem. Rev.* **2004**, *104*, 939.
[32] J.-U. Rohde, J.-H. In, M. H. Lim, W. W. Brennessel, M. R. Bukowski, A. Stubna, E. Münck, W. Nam, L. Que, Jr., *Science* **2003**, *299*, 1037.
[33] M. R. Bukowski, P. Comba, A. Lienke, C. Limberg, C. Lopez de Laorden, R. Mas-Balleste, M. Merz, L. Que, Jr., *Angew. Chem.* **2006**, *118*, 3524; *Angew. Chem. Int. Ed.* **2006**, *45*, 3446.
[34] O. Reinaud, P. Capdevielle, M. Maumy, *Synthesis* **1990**, 612.
[35] O. Reinaud, P. Capdevielle, M. Maumy, *J. Chem. Soc. Chem. Commun.* **1990**, 566.
[36] P. Capdevielle, D. Sparfel, J. Baranne-Lafont, N. K. Cuong, M. Maumy, *J. Chem. Soc. Chem. Commun.* **1990**, 565.
[37] P. Capdevielle, M. Maumy, *Tetrahedron Lett.* **1982**, *23*, 1573.
[38] O. Reinaud, P. Capdevielle, M. Maumy, *J. Mol. Catal.* **1991**, *68*, 13.
[39] W. Buijs, P. Comba, D. Corneli, H. Pritzkow, *J. Organomet. Chem.* **2002**, *641*, 71.
[40] J. P. Evans, K. Ahn, J. P. Kliman, *J. Biol. Chem.* **2003**, *278*, 49691.
[41] T. Kamachi, N. Kihara, Y. Shiota, K. Yoshizawa, *Inorg. Chem.* **2005**, *44*, 4226.
[42] K. Yoshizawa, Y. Shiota, *J. Am. Chem. Soc.* **2006**, *128*, 9873.
[43] S. Miertus, E. Scrocco, J. Tomasi, *Chem. Phys.* **1981**, *55*, 117.
[44] V. Barone, M. Cossi, *J. Phys. Chem. A* **1998**, *102*, 1995.
[45] A. Klamt, G. Schürmann, *J. Chem. Soc. Perkin Trans. 2* **1993**, 799.
[46] J. A. Pople, M. Head-Gordon, K. Raghavachari, *J. Chem. Phys.* **1987**, *87*, 5968.
[47] J. Cizek, *Adv. Chem. Phys.* **1969**, *14*, 35.
[48] G. D. Purvis, R. J. Bartlett, *J. Chem. Phys.* **1982**, *76*, 1910.
[49] G. E. Scuseria, C. L. Janssen, H. F. Schaefer, *J. Chem. Phys.* **1988**, *89*, 7382.
[50] G. E. Scuseria, H. F. Schaefer, *J. Chem. Phys.* **1989**, *90*, 3700.
[51] M. J. Frisch, G. W. Trucks, H. B. Schlegel, G. E. Scuseria, M. A. Robb, J. R. Cheeseman, J. A. Montgomery, Jr., T. Vreven, K. N. Kudin, J. C. Burant, J. M. Millam, S. S. Iyengar, J. Tomasi, V. Barone, B. Mennucci, M. Cossi, G. Scalmani, N. Rega, G. A. Petersson, H. Nakatsuji, M. Hada, M. Ehara, K. Toyota, R. Fukuda, J. Hasegawa, M. Ishida, T. Nakajima, Y. Honda, O. Kitao, H. Nakai, M. Klene, X. Li, J. E. Knox, H. P. Hratchian, J. B. Cross, V. Bakken, C. Adamo, J. Jaramillo, R. Gomperts, R. E. Stratmann, O. Yazyev, A. Austin, R. Cammi, C. Pomelli, J. W. Ochterski, P. Y. Ayala, K. Morokuma, G. A. Voth, P. Salvador, J. J. Dannenberg, V. G. Zakrzewski, S. Dapprich, A. D. Daniels, M. C. Strain, O. Farkas, D. K. Malick, A. D. Rabuck, K. Raghavachari, J. B. Foresman, J. V. Ortiz, Q. Cui, A. G. Baboul, S. Clifford, J. Cioslowski, B. B. Stefanov, G. Liu, A. Liashenko, P. Piskorz, I. Komaromi, R. L. Martin, D. J. Fox, T. Keith, M. A. Al-Laham, C. Y. Peng, A. Nanayakkara, M. Challacombe, P. M. W. Gill, B. Johnson, W. Chen, M. W. Wong, C. Gonzalez, J. A. Pople, *Gaussian 03*, *Revision B.03*, *Vol.* Gaussian Inc., Wallingford CT, **2003**.
[52] *JAGUAR 5.5*, Schrödinger Inc., Portland, OR.
[53] C. Lee, W. Yang, R. G. Parr, *Phys. Rev. B* **1988**, *37*, 785.
[54] A. D. Becke, *J. Chem. Phys.* **1993**, *98*, 5648.
[55] T. H. Dunning, Jr., P. J. Hay in *Modern Theoretical Chemistry, Vol. 3* (Ed.: H. F. Schaefer III), Plenum, New York, **1976**, pp. 1.
[56] P. J. Hay, W. R. Wadt, *J. Chem. Phys.* **1985**, *82*, 270.
[57] W. R. Wadt, P. J. Hay, *J. Chem. Phys.* **1985**, *82*, 284.
[58] P. J. Hay, W. R. Wadt, *J. Chem. Phys.* **1985**, *82*, 299.
[59] R. Ditchfield, W. J. Hehre, J. A. Pople, *J. Chem. Phys.* **1971**, *54*, 724.
[60] A. Schaefer, H. Horn, R. Ahlrichs, *J. Chem. Phys.* **1992**, *97*, 2571.
[61] A. Schäfer, C. Huber, R. Ahlrichs, *J. Chem. Phys.* **1994**, *100*, 5829.
[62] P. Flükiger, H. P. Lüthi, S. Portmann, J. Weber, *MOLEKEL 4.3*, Swiss Center for Scientific Computing, Manno, Switzerland, **2000**.
[63] S. Portmann, H. P. Lüthi, *CHIMIA* **2000**, *54*, 766.
[64] M. T. Cancès, B. Mennucci, J. Tomasi, *J. Chem. Phys.* **1997**, *107*, 3032.
[65] M. Cossi, B. Barone, B. Mennucci, J. Tomasi, *Chem. Phys. Lett.* **1998**, *286*, 253.
[66] B. Mennucci, J. Tomasi, *J. Chem. Phys.* **1997**, *106*, 5151.
[67] M. Cossi, G. Scalmani, N. Rega, V. Barone, *J. Chem. Phys.* **2002**, *117*, 43.
[68] The calculations reveal that this step (formation of the active oxidant) is endothermic by 488.7 kJ mol^{-1}, that is, this is the rate-limiting step and explains why this species was not detected. The endothermicity of this step was obtained from the energy difference between the reactant ^{2}**1** and the two products ^{3}**2** and TMA$^{+\bullet}$. With the product computed as an adduct the reaction energy decreases to the more realistic value of 185.8 kJ mol^{-1} at the Jaguar B3LYP/BSI level.

 © 2008 Wiley-VCH Verlag GmbH & Co. KGaA, Weinheim

[69] N. Kitajima, T. Koda, Y. Iwata, Y. Moro-oka, *J. Am. Chem. Soc.* **1990**, *112*, 8833.
[70] N. Kitajima, Y. Moro-oka, *Chem. Rev.* **1994**, *94*, 737.
[71] O. Kahn, *Molecular Magnetism*, Wiley, New York, **1993**.
[72] C. Würtele, E. Gaoutchenova, K. Harms, M. C. Holthausen, J. Sundermeyer, S. Schindler, *Angew. Chem.* **2006**, *118*, 3951; *Angew. Chem. Int. Ed.* **2006**, *45*, 3867.
[73] Note that the UB3LYP refinement of Cu^{III}=O converges to a closed-shell species.
[74] J. M. Meyer, *Comm. Inorg. Chem.* **1998**, *8*, 125.
[75] C. M. Barthelt, L. Ridder, A. J. Mulholland, J. N. Harvey, *J. Am. Chem. Soc.* **2005**, *127*, 12900.
[76] In the mechanism of the related Fe=O-catalyzed aromatic hydroxylation by P450 two orientations of benzene with respect to the metal–oxo group have been described (see Ref. [75]). Here, we describe an intramolecular process in which only one of the orientations is possible., Vol.
[77] Because ^{3}**2** is the ground state for the reactant all energy barriers are given with respect to the ground state regardless of the spin surfaces.
[78] P. Spuhler, M. C. Holthausen, *Angew. Chem.* **2003**, *115*, 6143; *Angew. Chem. Int. Ed.* **2003**, *42*, 5961.
[79] A. Fiedler, D. Schröder, S. Shaik, H. Schwarz, *J. Am. Chem. Soc.* **1994**, *116*, 10734.
[80] S. Shaik, D. Danovich, A. Fiedler, D. Schröder, H. Schwarz, *Helv. Chim. Acta* **1995**, *78*, 1393.
[81] D. Schröder, S. Shaik, H. Schwarz, *Acc. Chem. Res.* **2000**, *33*, 139.
[82] S. Shaik, H. Hirao, D. Kumar, *Acc. Chem. Res.* **2007**, *40*, 532.
[83] D. Schröder, M. C. Holthausen, H. Schwarz, *J. Phys. Chem. B* **2004**, *108*, 14407.
[84] Y. Shiota, K. Yoshizawa, *J. Chem. Phys.* **2003**, *118*, 5872.
[85] M. Kondo, K. Yoshizawa, *Chem. Phys. Lett.* **2003**, *372*, 519.
[86] The intermediates and the transition state on the other spin surfaces have not been converged to the correct wave function and are, therefore, not included.
[87] A. Kunishita, J. Teraoka, J. D. Scanlon, T. Matsumoto, M. Suzuki, C. J. Cramer, S. Itoh, *J. Am. Chem.Soc.* **2007**, *129*, 7248.
[88] H. Li, H. Jemsen, *J. Comput. Chem.* **2004**, *25*, 1449.
[89] D. F. Raffa, G. A. Rickard, A. Rauk, *J. Biol. Inorg. Chem.* **2007**, *12*, 147.
[90] J. P. Holland, J. C. Green, J. R. Dilworth, *Dalton Trans.* **2006**, 783.
[91] L. Barrio, J. M. Campos-Martin, J. L. G. Fierro, *J. Phys. Chem. A* **2007**, *111*, 2166.
[92] W. H. Lam, E. C. Cheng, V. W. Yam, *Inorg. Chem.* **2006**, *45*, 9434.
[93] A. A. Jarzecki, A. D. Anbar, T. G. Spiro, *J. Phys. Chem. A* **2004**, *108*, 2726.
[94] K. Sugimori, T. Shuku, A. Sugiyama, H. Nagao, T. Sakurai, K. Nishikawa, *Polyhedron* **2005**, *24*, 2671.
[95] J. M. H. Lo, M. Klobukowski, *Inorg. Chim. Acta* **2003**, *353*, 15.
[96] See Supporting Information for the computed energies of the solvated species with different solvation models in comparison with the gas-phase energies.
[97] The transition state on the ^{1}**3** surface could not be successfully optimized by using the CPCM solvation model.
[98] D. L. Reid, G. V. Shustov, D. A. Armstrong, A. Rauk, M. N. Schuchmann, M. S. Akhlaq, M. Shahid, C. von Sonntag, *Phys. Chem.* **2002**, *4*, 2965.
[99] S. Wolfe, C.-K. Kim, K. Yang, N. Weingerg, Z. Shi, *J. Am. Chem. Soc.* **1995**, *117*, 4240.
[100] S. Wolfe, Z. Shi, K. Yang, S. Ro, N. Weingerg, C.-K. Kim, *Can. J. Chem.* **1998**, *76*, 114.
[101] S. P. de Visser, F. Ogliaro, N. Harris, S. Shaik, *J. Am. Chem. Soc.* **2001**, *123*, 3037.
[102] A. Bassan, M. R. A. Blomberg, P. E. M. Siegbahn, *Chem. Eur. J.* **2003**, *9*, 4055.
[103] A. Bassan, M. R. A. Blomberg, P. E. M. Siegbahn, *J. Biol. Inorg. Chem.* **2004**, *9*, 439.
[104] A. Bassan, M. R. A. Blomberg, P. E. M. Siegbahn, L. Que, Jr., *Chem. Eur. J.* **2005**, *11*, 692.
[105] D. Quinonero, K. Morokuma, D. G. Musaev, K. Morokuma, R. Mas-Balleste, L. Que, Jr., *J. Am. Chem. Soc.* **2005**, *126*, 6548.
[106] J. N. Harvey, *Annu. Rep. Prog. Chem. Sect. C* **2006**, *102*, 203.
[107] P. E. M. Siegbahn, T. Borowski, *Acc. Chem. Res.* **2006**, *39*, 729.
[108] S. Shaik, D. Kumar, S. P. De Visser, A. Altum, W. Thiel, *Chem. Rev.* **2005**, *105*, 2279.
[109] B. Meunier, S. P. de Visser, S. Shaik, *Chem. Rev.* **2004**, *104*, 3947.
[110] B. F. Gherman, C. J. Cramer, *Inorg. Chem.* **2004**, *43*, 7281.
[111] E. Ruiz, S. Alvarez, A. Rodriguez-Fortea, P. Alemany, Y. Pouillon, C. Massobrio, *Magnetism: Molecules to Materials Vol. 3* (Eds.: J. S. Miller, M. Drillon), Wiley-VCH, Weinheim, **2001**.
[112] P. E. M. Siegbahn, *J. Biol. Inorg. Chem.* **2006**, *11*, 695.
[113] F. Neese, *J. Inorg. Biochem.* **2006**, *100*, 716.
[114] F. Neese, *J. Biol. Inorg. Chem.* **2006**, *11*, 702.
[115] A. Ghosh, *J. Biol. Inorg. Chem.* **2006**, *11*, 712.
[116] T. J. Lee, A. P. Rendell, P. R. Taylor, *J. Phys. Chem.* **1990**, *94*, 5463.
[117] S. Niu, M. B. Hall, *J. Phys. Chem. A* **1997**, *101*, 1360.
[118] B. G. Johnson, P. M. W. Gill, J. A. Pople, *J. Chem. Phys.* **1993**, *98*, 5612.
[119] Therefore, the reported barrier for the model complex using DFT, QCISD and CCSD calculations does not include ZPE or free-energy corrections.
[120] M. Atanasov, P. Comba, B. Martin, V. Müller, G. Rajaraman, H. Rohwer, S. Wunderlich, *J. Comput. Chem.* **2006**, *27*, 1263.
[121] R. K. Szilagyi, M. Metz, E. I. Solomon, *J. Phys. Chem. A* **2002**, *106*, 2994.
[122] S. DeBeer George, L. Basumallick, R. K. Szilagyi, D. W. Randall, M. G. Hill, A. M. Nersissian, J. S. Valentine, B. Hedman, K. O. Hodgson, E. I. Solomon, *J. Am. Chem. Soc.* **2003**, *125*, 11314.
[123] R. J. Deeth, *J. Chem. Soc. Dalton Trans.* **2001**, 664.
[124] J. H. Harvey, *Struct. Bonding* **2004**, *112*, 151.
[125] J. K. Kang, C. B. Musgrave, *J. Chem. Phys.* **2001**, *115*, 11040.
[126] B. J. Lynch, P. L. Fast, M. Harris, D. G. Truhlar, *J. Phys. Chem. A* **2000**, *104*, 4811.
[127] Note that it is not unlikely that the B3LYP calculations are more reliable than the CCSD results because of the use of a minimal basis set for the CCSD calculations.

Received: June 6, 2007
Published online: September 28, 2007

 © 2008 Wiley-VCH Verlag GmbH & Co. KGaA, Weinheim